Research paper

Mechanical changes in metals caused by transmission of explosive shock waves and a consideration to fragmentation energy in cylinder explosions

Tetsuyuki Hiroe †, Kazuhito Fujiwara, Hidehiro Hata, and Kenjiro Watanabe

Department of Advanced Mechanical Systems, Graduate School of Science and Technology, Kumamoto University, 2-39-1 Kurokami, Kumamoto 860-8555, JAPAN
† Corresponding address: hiroe@gpo.kumamoto-u.ac.jp

Received: March 17, 2008 Accepted: June 19, 2008

Abstract

Explosive driven fracture such as fragmentation or spallation in a structural body will be preceded by a strong compression process, and precompression effects on the state of the material are clearly important to understand the following shock-induced damages or failures. In this study, incident shock waves in plate specimens of 304 stainless steel and aluminum alloy A5052 were generated by plane detonation waves in the high explosive PETN initiated using wire-row explosion techniques, and the compressed specimens were successfully recovered without severe damages due to tensile stress states with use of momentum trap method. A hydro code, Autodyn-2D was applied to determine test conditions: thicknesses of explosives, air-layer attenuators as necessary, specimens and momentum traps and to evaluate experimental results, simulating time-histories of stress waves in the layers of the test assembly. Microhardness distributions in cross-sections, tensile strength, fracture ductility and flow stresses were measured for the recovered specimens, using miniature tensile and compression test pieces machined from them. They were compared with those of specimens from unloaded virgin plates, revealing significant increase of hardness, tensile strength and flow stresses and unique changes of elongation and ductility for shocked specimens depending on the intensities of the transmitted compression waves and the materials. The results were effectively applied to take the precompression effects into consideration of the strain-rate dependency of fragmentation energy values derived from the previous explosion tests for cylinders of the same materials using a fragmentation model.

Keywords: Mechanical properties, Shock wave transmission, Momentum trap, Cylinder explosion, Fragmentation energy

1. Introduction

Dynamic fracture induced by explosive loadings occurs as spallation or fragmentation when an excessive tensile stress is created by the reflection of a strong shock wave at a free surface of a plate structure or by the interior rapid expansion of detonation gas after shock incidence and sequential reflection in the wall of a casing structure. Such explosively driven damages are typically initiated by impacts between solids and detonation gases and strong compressive stress waves are created and transmitted through the bodies prior to the terminal tensile deformation and fracture of structures, but usually such preceded processes have not been taken into the evaluation of posterior fractural phenomena.

In this study, explosively shocked plate specimens of aluminum A5052 and 304 stainless steel were successfully recovered without a large amount of damages due to the reflected expansion waves using momentum traps designed with help of numerical simulations. Wire explosion techniques [1), 2)] to produce diverging and planar detonation waves in the powder high explosive pentaerythritoltetranitrate (PETN) developed by authors for the studies on spall fracture of plates [3)] and uniform expansion and fragmentation of cylinders [4), 5)] of aluminum alloys and a stainless steel were also applied as an initiation method for shock loading of the specimens. Observed mechanical properties of the recovered specimens indicated noticeable changes from those of the virgin materials, giving some considerations on the fragmentation energy based on a fragmentation model and the previous fragment data [6)] for exploded cylinders of the same materials.

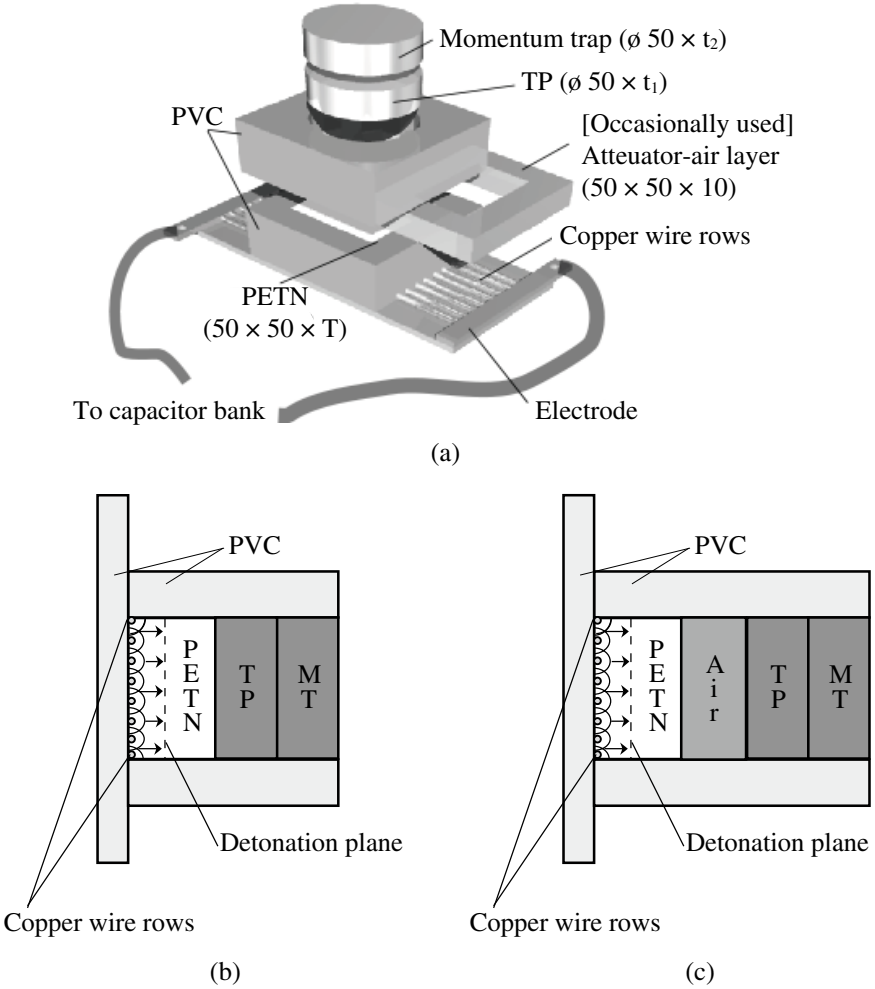

Fig. 1 (a): Schematics of test assembly for recovery of explosively compressed circular plate specimens, and (b), (c): two types of explosive loadings, direct incidence type and attenuator (air layer) inserted type.

2. Experimental procedure

Explosively loading experiments were performed using the explosion test facilities at the Shock Wave and Condensed Matter Research Center, Kumamoto University.

Figure 1 (a) – (c) illustrates schematics of overall test assembly (a) for recovery of explosively compressed circular plate specimens, and two types of explosive loadings, direct incidence type (b) and attenuator (air layer) inserted type (c). Typical loading type (c) consists of four layers of a PETN slab packed to 0.93-0.95 g·cm^{-3} with attached parallel copper wire-rows (wire diameter: 175 μm, the ratio of PETN thickness to wire interval: 1.3-1.5) for generation of planar detonation [1), 2)], an air layer as an attenuator (AT), a circular plate specimen (TP) of aluminum alloy JIS A5052 or 18 Cr-8 Ni stainless steel (JIS SUS304), and a circular momentum trap plate (MT) of the same material as specimen. The PETN are filled up to 15 mm and 20 mm thick for A5052 and SUS304 respectively. The air layer AT is inserted in order to decrease or adjust the intensity of shock pressure transmitted to the specimen. The thickness of 10 mm is designated from numerical experiments shown later. The contact surfaces of specimens and the momentum traps are lapped to superfine finish. A planar detonation front is produced in the PETN layer immediately after simultaneous explosion of wire-rows with use of an impulsive discharge current from a capacitor bank of 40 kV, 12.5 μF and a triangular-type planar pressure pulse transfers into TP and MT. It is expected that the TP would be recovered without severe damages with effect of the MT attachment. The thicknesses t_1 and t_2 of provided TP and MT are 10, 12 mm: two kinds of combinations for A5052 and 10, 15 mm: four kinds for SUS304, and then the combinations are expressed as TPt_1MTt_2 or TPt_1MTt_2AT10. All the explosive test conditions were designated by the following numerical results and they are summarized in Table 1.

Mechanical property tests for recovered precompressed plate specimens were conducted as typically shown for SUS304 with photos and illustrations in Fig. 2: (a) measurement locations at an interval of 1mm axially and 5mm radially for Vickers microhardness Hv, (b) miniature tensile specimen with the minimum diameter of 2 mm and (c) small column specimens for compression tests with a diameter of 5 mm and 7.5 mm length. They were produced by electro-discharge machining from the plates. The vertical cross-section of the recovered specimens is surface-finished and Hv values are measured using a

Table 1 Combinations of thicknesses for recovery tests of explosively precompressed plate specimens (unit: mm).

Materials of specimen	High explosive PETN (T)	Direct incident cases		Attenuator inserted cases		
		Test piece TP (t_1)	Momentum trap MT (t_2)	Test piece TP (t_1)	Attenuator AT	Momentum trap MT (t_2)
A5052	15	10	12	10	10	12
SUS304	20	10	10 15	10	10	10 15
		15	10 15	15	10	10 15

Remarks: T, t_1 and t_2 correspond with those in Fig. 1(a).

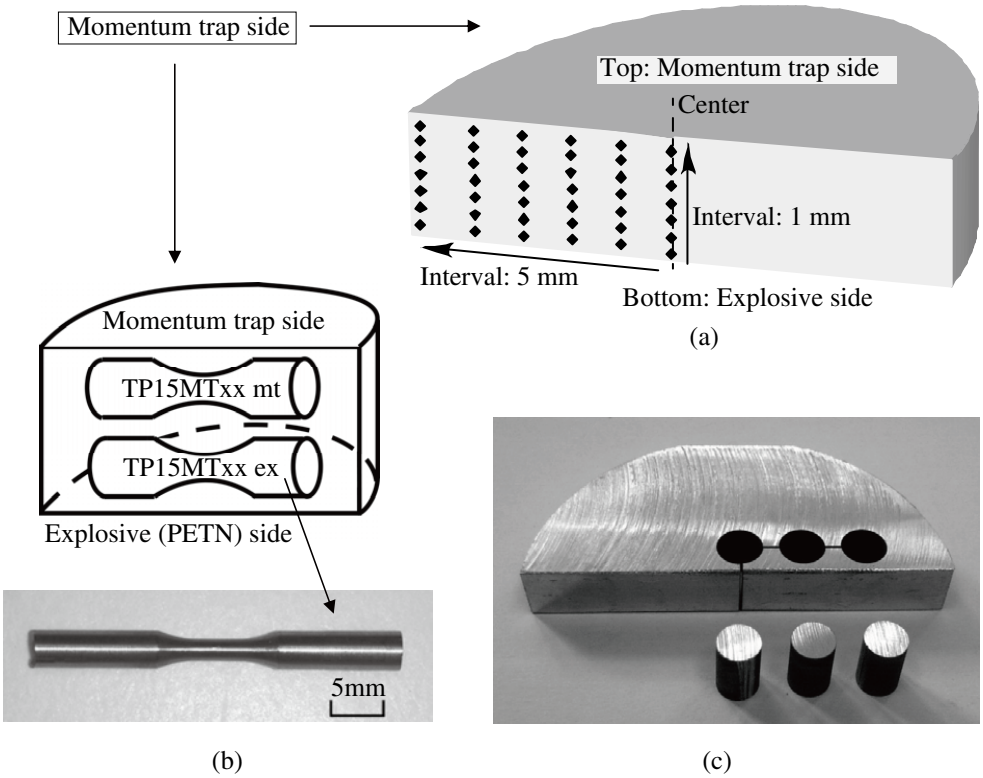

Fig. 2 Mechanical property test speciments for SUS304 of recovered precompressed specimen plates, (a) measurement locations for Vickers microhardness, (b) miniature tensile specimen and (c) small column specimens.

load of 0.98 N and 15 s duration for all the plate specimens. Tensile and compression tests are performed using Shimadzu AG-25TB Autograph and full digital servo-hydraulic testing system FHF-EG50kN-10L.

3. Numerical stress histories in the test assembly

Numerical simulations were performed for all the experiments using a hydro code: Autodyn 2D based on finite difference method (FDM), where the Steinberg-Guinan model [7] is adopted for the constitutive equations for metals.

Figure 3 represent typical two dimensional axisymmetric finite difference model for the test assembly of the attenuator inserted type. The metallic solids are divided into ring elements with 0.2 × 0.2 mm sections using Lagrange grid and gap elements are inserted between the specimen and momentum trap plates. A squarely installed PETN is

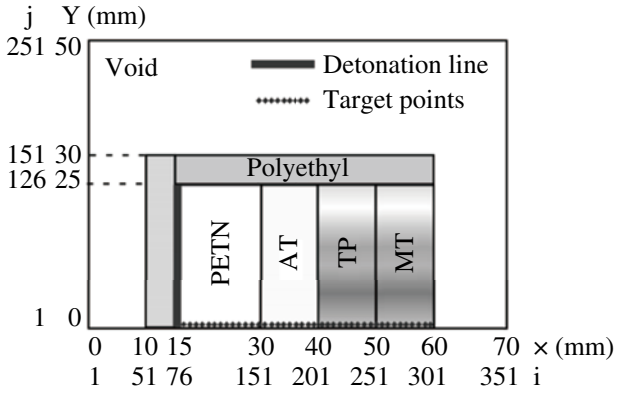

Fig. 3 Typical two dimensional axisymmetric finite difference model for test assembly (attenuator inserted type), using a hydro code, Autodyn 2D.

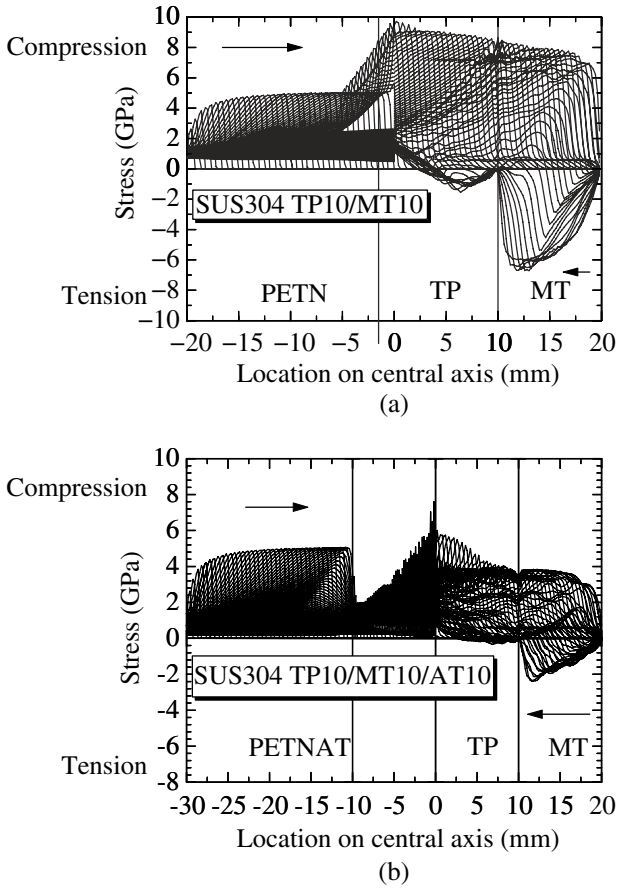

Fig. 4 Typical comparison of numerical time histories of spatial stress distributions between (a) in the direct incidence type test assembly for TP10 / MT10 (elapsed time: 0-10 μs) and (b) in the attenuator inserted type for TP10 / MT10 / AT10 (elapsed time: 0-14.1 μs) both of SUS304.

assumed to be a circular plate and the detonation initiates simultaneously at the bottom surface of the explosive. The stresses were evaluated at the central target points.

Figure 4 (a), (b) shows typical numerical time-histories of spatial distributions of normal stress in the test assembly layers for (a) direct incidence type TP10 / MT10 and (b) an attenuator inserted type AT10 / TP10 / MT10 both of SUS304. Damage criteria are not adopted in these calculations. It is seen that triangular compressive stress waves propagate through TP and MT, and the reflected tensile stress waves generated in MT do not transfer into TP for both cases. The effect of attenuator, air layer with the thickness of 10 mm is apparently shown in (b), and the incident shock pressure in TP is 53.8 % of that in case without AT, which almost corresponds to the numerical pressure reduction rate of 59.7 % in cylinder explosion tests [3), 6)] with an air layer between cylinder specimen and the inner explosive column as shown in Fig. 9 (a) later. Other numerical study reproduced experimental spall failure in MT using a damage criterion.

4. Precompressional effects on mechanical properties

Recovery tests of explosively compressed specimens were successfully performed inside a cushion-filled

Fig. 5 A typical photo of damaged free surface of recovered momentum trap MT (left) and momentum side surface of recovered test specimen TP (right) for direct incidence type test (TP10 / MT15) of SUS304.

chamber without secondary damages in TP and MT. Macroscopic severe damages were not observed in almost all the TP specimens, but spall or scab damages were produced in most of MT palates, as typically shown in Fig. 5. Such damages in MT are similar to those [3)] previously observed experimentally and successfully simulated numerically using the spall strength of 3.9 GPa for SUS304.

The cross-section of recovered specimens revealed no presence of macroscopic cracks and the microhardness of the plates was measured.

Figure 6 shows typical comparisons of Vickers microhardness distributions in the cross-section of a recovered precompressed plate specimens and virgin plates of both loading types for SUS304 (TP10 / MT15, TP10 / MT15 / AT10) and A5052 (TP10 / MT12, TP10 / MT12 / AT10). The tendency is common for other cases and all the results revealed a remarkable increase in hardness in comparison with those of virgin materials and the effect of the air-layer attenuator or the intensity of precompression load is more obvious for SUS304 than for A5052.

Miniature tensile specimens were loaded to break under 2 mm·min^{-1} chuck velocity.

Figure 7 (a1)-(c) shows typical photos of tested miniature tensile specimens for (a1) TP10 / MT10 / AT10 of SUS304 and (a2) TP10 / MT12 of A5052, and comparisons of average data of tensile strength σ_B , reduction of area (RA) Φ and elongation λ for virgin and explosively precompressed materials of SUS304 (b) and A5052 (c). In the tensile tests, σ_B, λ and Φ were obtained measuring breaking load, elongated length between two Vickers indentations with distances of gauge length of 5 mm and minimum section area. It is well known that the empirical proportional relation between tensile strength [MPa] and microhardness [Hv] written as equation (1) and the fracture ductility ε_f is also estimated from RA using the following equation (2), which is sometimes more effective to evaluate practical local ductile fracture than averaged elongation λ.

$$\sigma_B = C \cdot Hv \tag{1}$$

$$\varepsilon_f = \ln\left(\frac{1}{1-\Phi}\right) \tag{2}$$

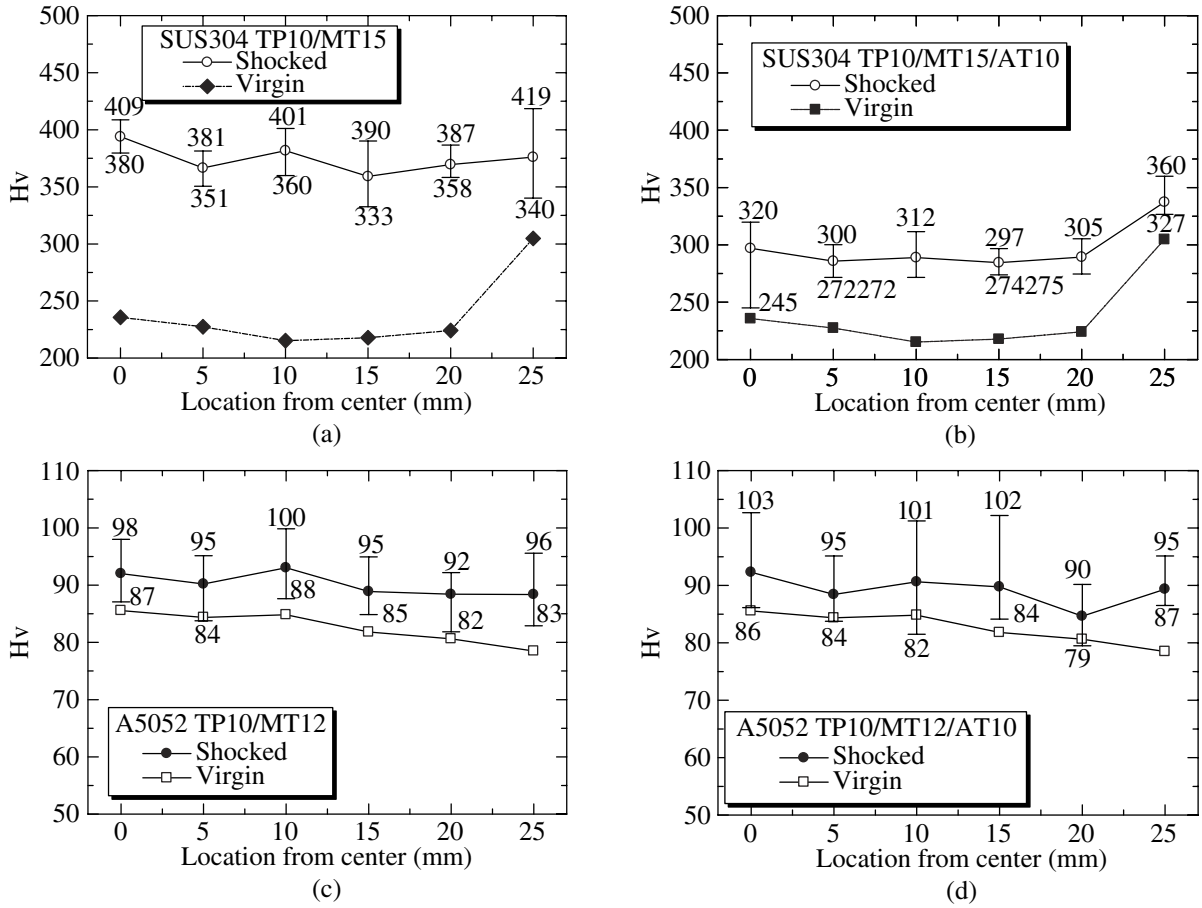

Fig. 6 Typical comparisons of measurement results of Vickers microhardness distributions in the cross- section of a recovered precompressed specimen and virgin plates of both loading types for SUS304 (TP10 / MT15, TP10 / MT15 / AT10) and A5052 (TP10 / MT12, TP10 / MT12 / AT10).

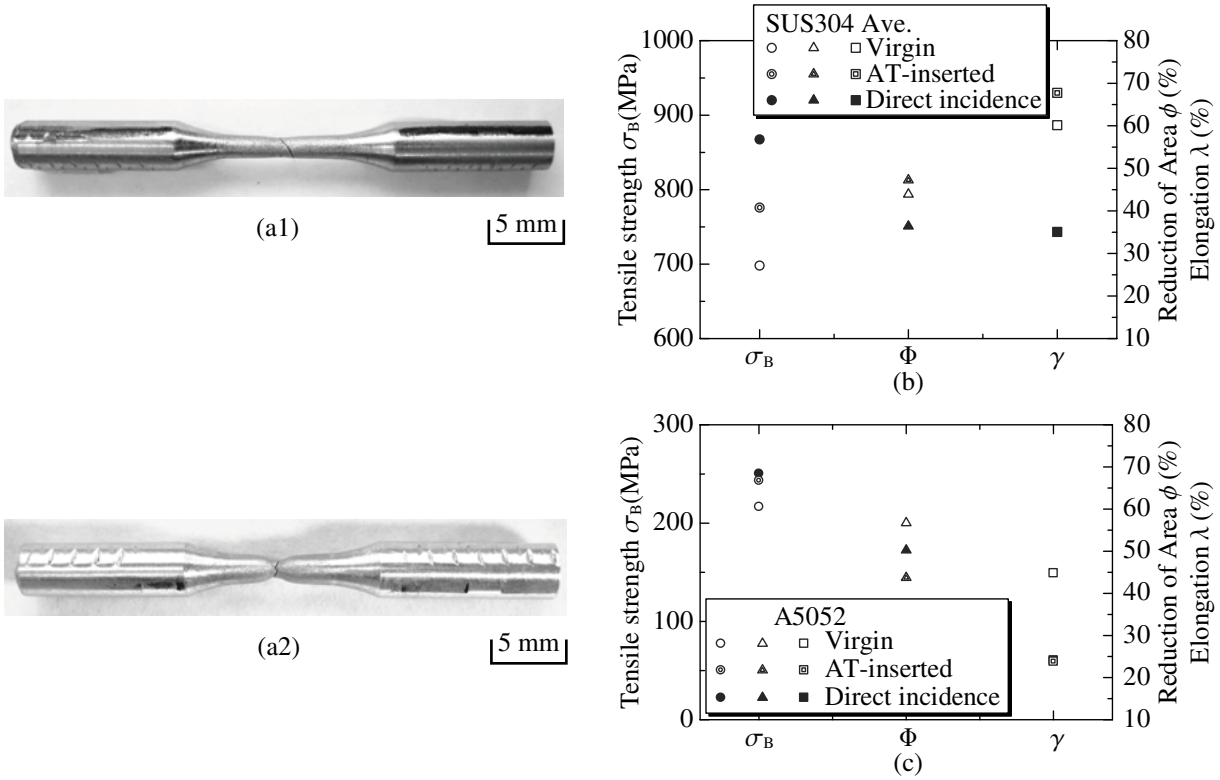

Fig. 7 Typical photos of tested miniature tensile specimens for (a1) TP10 / MT10 / AT10 of SUS304 and (a2) TP10 / MT12 of A5052, and comparisons of average data of tensile strength σ_B, reduction of area θ and elongation λ for virgin and explosively precompressed materials (attenuator AT inserted and direct incidence) of SUS304 (b) and A5052 (c).

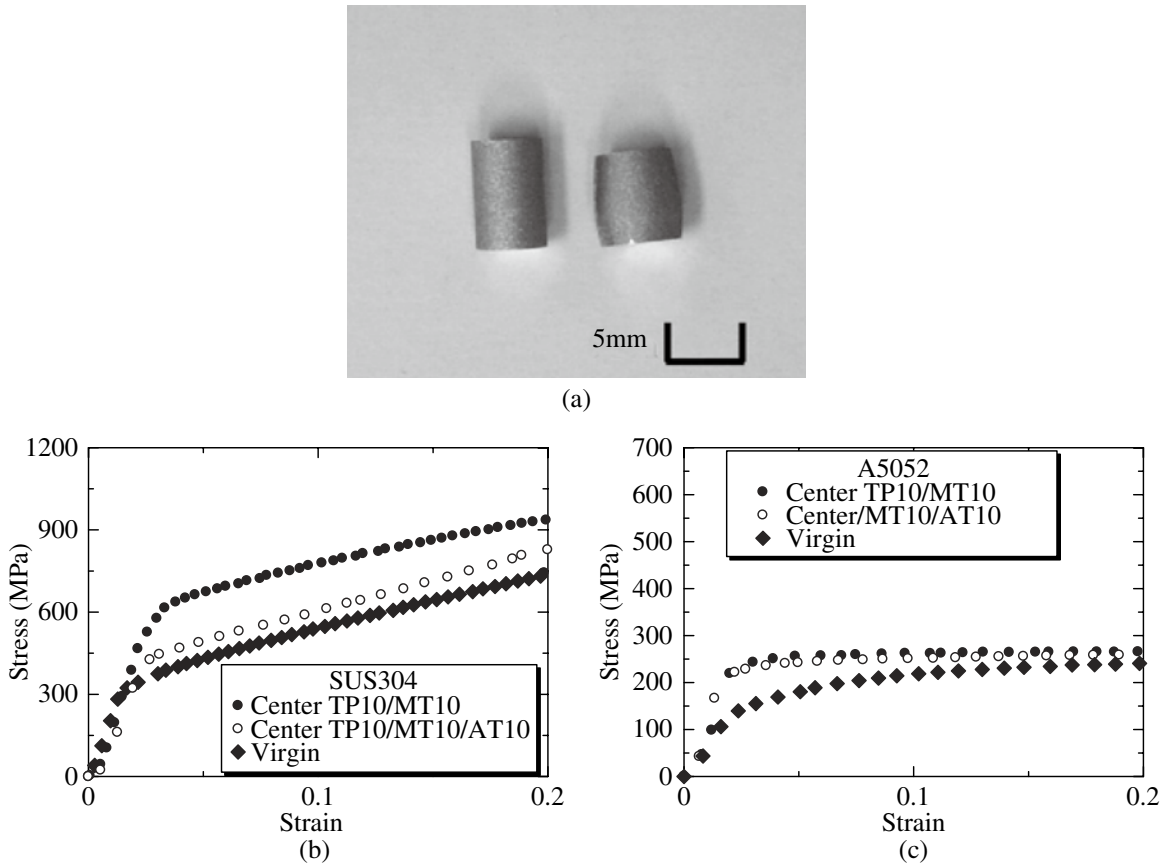

Fig. 8 Typical photos of compression test specimens before (left, outer location) and after (right) the test for TP10 / MT12 / AT10 of A5052, and comparisons of average data of compressive stress-strain curves for virgin and explosively precompressed materials from TP10 / MP10 (direct incidence) and TP10 / MT10 / AT10 (attenuator inserted) of SUS304 (b) and A5052 (c).

Tensile tests results indicated larger σ_B values and smaller Φ and λ values for precompressed materials than those for virgin ones and $C = 2.3 - 2.9$ (average based) in equation (1) for both materials, but only for Φ and λ values of SUS304 there appeared no difference or opposite tendency between virgin material and the material precompressed through an air-layer attenuator.

Figure 8 represents typical photos of compression test specimens before and after the test showing barrel type deformation due to the friction at the loaded and supported surfaces for TP10 / MT12 / AT10 of A5052, and comparisons of compressive stress-strain curves for virgin and explosively precompressed specimens from TP10 / MP10 and TP10 / MT10 / AT10 of SUS304 (b) and A5052 (c). The stress-strain curves reveal obviously different precompression effects between two materials indicating that A5052 has a gradually decreasing strain-hardening characteristic, then the differences of stress levels in the stress-strain curves between virgin and shocked materials become smaller as the strain grows, and on the contrary, SUS304 which has a constant hardening characteristic shows stress-strain curves for precompressed materials upper shifted from that for virgin one. The attenuator inserted effect is distinctive for SUS304, but for A5052 both curves for shocked materials are almost same. This phenomenon seems also related with the different strain hardening for both materials. The stresses at the plastic strain of 20 %, $\sigma_{0.2}$ are adopted as reference flow stresses for both materials in the following discussion on fragmentation energy considering that the critical or fracture strain of exploded cylinders was 39-50 % [4] and the 20 % is near the average value of plastic deformation prior to fracture.

All the testes data for mechanical properties are summarized in Table 2.

5. Discussions on fragmentation energy of exploding cylinders

Our previous study [3] indicated the spall strength σ_{sp} values of plates shocked directly by plane detonation waves of PETN for A2024 and SUS304 are 262-308 MPa and 352-453 MPa respectively, which are twice to several times of static tensile strength σ_B. It has become obvious that such large increase of dynamic strength involves not only well known strain-rate effect but also basic growth of σ_B or hardness due to precompression learned in this study. Such precompression effects seem to be common to all the dynamic fracture phenomena driven by explosive loads or intensive shock waves. Hereafter obtained test results are applied to other previous studies [4) ~ 6)] on fragmentation of exploding cylinders of A5052 and SUS304 driven by uniformly expanding detonation waves in inserted PETN column.

Figure 9 represents (a) a schematic of test assembly for previously performed explosion test of cylinders driven by uniformly expanding detonation waves in inserted PETN column initiated at the central axis using a wire explo-

Table 2 Summary of mechanical properties for precompressed and virgin specimens and related calculations for fragmentation energy.

Combination of TP, AT and MT for compression tests	Hv**	Tensile tests				Compression tests			Fr.E*
		σ_B (MPA)	λ (%)	Φ (%)	ε_f (%)	$\sigma_{0.2}$ (MPa9) Inner	Mid.	Outer	$\Gamma\cdot\Gamma_0^{-1}$ (%)
A5052 (Direct incidence)									
(Virgin plate)	83	216	44.8	56.7	0.84	—	241	—	100
TP10 / MT12	90	251	24.1	50.2	0.70	266	264	263	91
A5052 (Attenuator inserted)									
TP10 / MT12 / AT10	89	243	23.8	43.7	0.57	258	259	260	74
SUS304 (Direct incidence)									
(Virgin plate)	238	698	60.0	43.9	0.58	—	737.6	—	100
TP10 / MT10	305	913	21.0	32.4	0.39	936	978	1008	89
TP10 / MT15	350	831	51.6	40.3	0.52	977	970	968	118
TP15 / MT10 ex†	408	824	40.7	41.0	0.53	991	948	959	119
TP15 / MT10 mt††		804	46.6	39.6	0.51				114
TP15 / MT15 ex†	319	926	14.5	30.8	0.37	1025	989	1016	87
TP15 / MT15 mt††		908	36.0	34.3	0.42				99
(Average data)	345	868	35.1	36.4	0.47	991	970	988	105
SUS304 (Attenuator inserted)									
TP10 / MT10 / AT10	310	810	77.4	53.6	0.77	828	838	823	149
TP10 / MT15 / AT10	297	767	55.9	43.6	0.57	864	856	864	116
TP15 / MT10 / AT10 ex†	426	781	73.1	46.0	0.62	808	777	797	115
TP15 / MT10 / AT10 mt††		777	73.0	52.2	0.74				137
TP15 / MT15 / AT10 ex†	341	766	60.4	42.9	0.56	851	822	829	110
TP15 / MT10 / AT10 mt††		755	66.6	45.4	0.60				118
(Average data)	343	776	67.7	47.3	0.64	835	815	823	124

Remarks: * $\Gamma \cdot \Gamma_0^{-1}$: Ratio of fragmentation energy Γ ($\propto \sigma_{0.2} \cdot \varepsilon_f$) of precompressed specimens to that of virgin materials Γ_0, **Hv: Micro Vickers hardness, ex†, mt††: test piece location data, see Fig. 2 (b), σ_B.: tensile strength, λ: elongation, Φ: reduction of area, ε_f: fracture ductility (= $\ln(1-\Phi)^{-1}$).

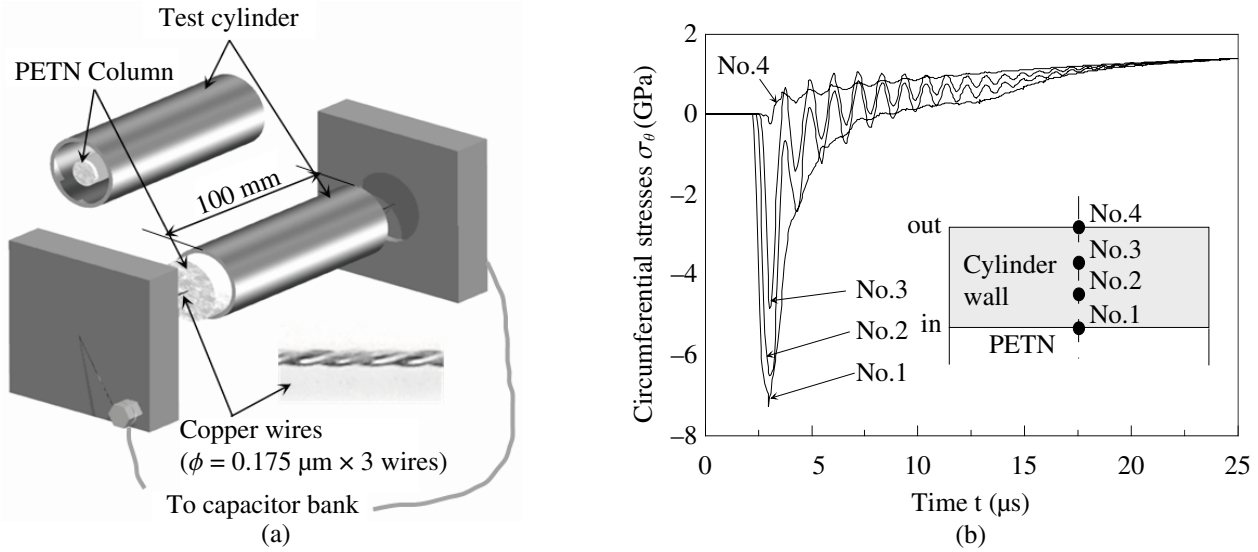

Fig. 9 (a) A schematic of test assembly for uniform explosion of cylinders and (b) a typical example[6] of numerical time-history of circumferential stresses (minus stress value means compression here) in the wall at the mid-length for a standard cylinder of SUS304 with fully charged PETN.

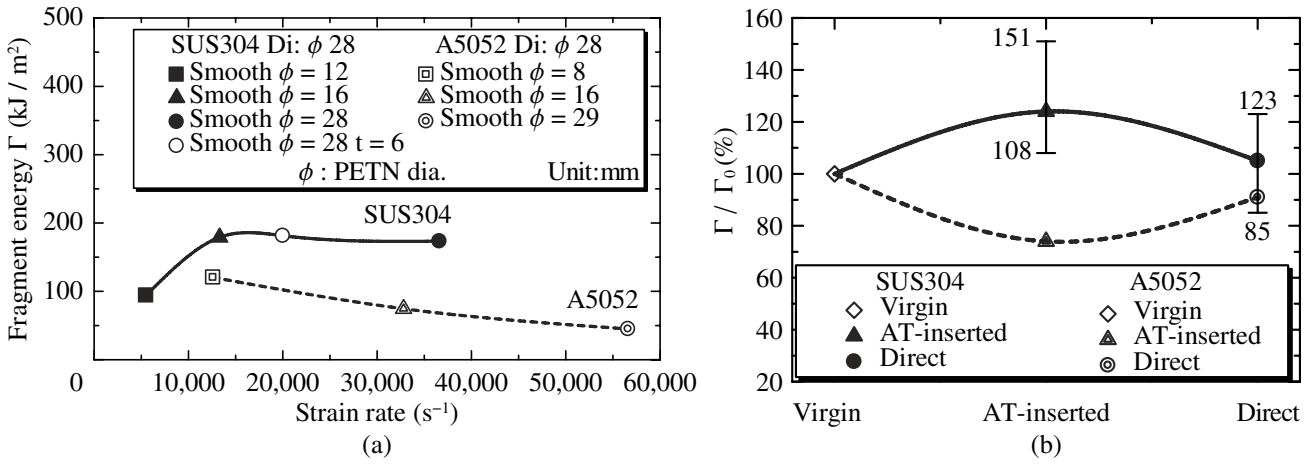

Fig. 10 (a) Relations [6] between the ratios of fragmentation energy values Γ calculated from Grady's model and strain rates for cylinders of SUS304 and A5052, and (b) the ratio of fragmentation energy Γ for precompressed materials to those Γ_0 of virgin materials vs. material processing corresponding to strain rates for the same materials estimated in this study.

sion technique and (b) a typical example [6] of numerical time-history of circumferential stresses in the wall at the mid-length for a standard cylinder of SUS304 with fully charged PETN. The standard cylinders with the sizes: length L inner diameter d_i wall thickness t of 100 × 29 × 3 mm (A5052) and 100 × 28 × 3 mm (SUS304) are tested, then in case that the PETN diameter ϕ is smaller than d_i, an air layer is inserted between the cylinder specimen and the PETN column as an attenuator. The numerical result of the direct incident case ($d_i = \phi$ or full charge) shows the incidence of strong compression wave and its oscillations prior to the growth of tensile stress in the wall. The reduction of PETN diameter decreases the precompression intensity or strain rate of exploding cylinders and the case of ϕ = 16 mm almost corresponds to the AT inserted type of test assembly for plates as to the reduction rate of precompression stress. The studies [4) ~ 6)] on fragmentation of exploding cylinders of A5052 and SUS304 had indicated that the fragmentation energy Γ values estimated from the Grady's fragmentation model [8] : equation (3) using strain-rate $\dot{\varepsilon}$ of expanding cylinders and measured average width s of recovered fragments differ depending on the amount of explosives or strain-rates as shown in Fig. 10(a).

$$\Gamma = \frac{\rho \dot{\varepsilon}^2 s^3}{24} \tag{3}$$

The fragmentation energy Γ of a material is often expressed [8] as a half of a product of yield stress σ_Y and critical crack opening displacement δ_C based on the assumption of non strain-hardening but in this study following equation (4) is obtained using $\sigma_{0.2}$ as a reference stress for strain-hardening materials instead of σ_Y on the assumption that δ_C is proportional to fracture ductility .

$$\Gamma = \sigma_{0.2} \cdot \delta_C / 2 \propto \sigma_{0.2} \cdot \varepsilon_f \tag{4}$$

Figure 10 (b) indicates the ratios of fragmentation energy Γ for precompressed materials to those Γ_0 of virgin materials vs. groups of material processing corresponding to strain rates for the same materials estimated from the equation (4). See Table 2 for all the calculated data. It is shown that the Γ values in Fig. 10 (a) obtained from the fragmentation model and the fragment measurement of exploded cylinders are not constant but increase or decrease depending on the subjected strain-rates related with the intensity of precompression, and it is suggestible that this overall tendency is basically similar to that of the Γ ratios in Fig. 10 (b) also depending on precompression processes of AT-inserted and direct loadings on the mechanical properties of precompressed plates in this study although cylinder fragmentation phenomenon must be affected by some other factors such as microstructural changes ignored here.

6. Conclusions

The plate specimens of A5052 and SUS304 precmpressed by planar detonation waves in PETN initiated using wire-row explosion technique were recovered without severe damages applying momentum trap method. Mechanical property tests of recovered specimens indicated the following results:

(1) Microhardness of precompressed materials increased and the growth behavior of tensile strength seemed to be related with the stress-strain characteristics of the materials
(2) Elongation, reduction of area, and fracture ductility of precompressed materials mostly decreased except SUS304 compressed with low intensity using an air-layer attenuator.
(3) The stresses at the strain of 0.2 for precompressed materials were adopted as reference flow stresses related with fragmentation energy, and the increase or decrease tendency of experimental fragmentation energy values due to precompression derived from previous cylinder explosion tests is basically similar to that estimated from the mechanical properties of recovered plates in this study.

Acknowledgement

This study was partially supported by the Foundation for the Promotion of the Industrial Explosive.

References

1) T. Hiroe, H. Matsuo, K. Fujiwara, M. Yoshida, S. Fujiwara, M. Miyata, S. Sakai, T. Fukano and T. Abe, Sci. Tech. Energetic Materials, 57, 49 (1996).
2) T. Hiroe, K. Fujiwara, H. Matsuo, Y. Araki and D. Nakayama, 15th International Conference on Structural Mechanics in Reactor Technology (SmiRT-15), Vol. VII, pp. 161 -168 (1999), Seoul.
3) T. Hiroe, K. Fujiwara, H. Matsuo and N. N. Thadhani, Fourth International Symposium on Impact Engineering, pp. 851-856 (2001), Kumamoto.
4) T. Hiroe, K. Fujiwara, T. Abe and M. Yoshida, 13th Biennial International Conference of the APS Topical Group on Shock Compression of Condensed Matter, pp. 465–472 (2003), Portland.
5) T. Hiroe, K. Fujiwara and H. Hata, 16th Dynamic Behavior Related to Security Applications (DYMAT) Meeting, pp. 159-167 (2005), Brussels.
6) T. Hiroe, K. Fujiwara, H. Hata, K and H. Takahashi, International Journal of Impact Engineering, (in print)
7) D. J. Steinberg, S. G. Cochran, and M. W. Guinan, J. Appl. Phys., 51, 1498 (1980).
8) D. E. Grady, and M. M. Hightower, “Shock-wave and high-strain-rate phenomena in materials”, 713 (1992), Marcel Dekker, Inc.

爆発衝撃波透過による金属の力学特性変化と円筒の爆発分裂エネルギーへの考察

廣江哲幸†，藤原和人，波多英寛，渡辺健次郎

構造体における爆薬駆動の分裂･剥離破壊などでは強い圧縮過程が先行する。したがって材料状態への先行圧縮の影響は、後続の衝撃波起因の損傷や破断を理解するために重要なことは明らかである。本研究では、304ステンレス鋼とアルミニウム合金A5052製の円板供試体に、線列爆発技術を用いて起爆させた高性能爆薬PETNの平面爆轟波による入射衝撃波を生成させ、モーメンタムトラップ法を適用することで、圧縮された供試体に引張応力による大きな損傷を発生させずに回収することに成功した。衝撃解析コードのAutodyn 2Dを用い、爆薬、必要に応じての空気層･緩衝材、試験体、モーメンタムトラップなどの厚さの決定や、試験装置各部における応力履歴のシミュレーションによる実験結果の評価を行った。回収供試体の断面のマイクロヴィッカース硬度計測を、また供試体から採取したミニチュアの引張･圧縮試験片を用いて引張強度、破壊延性及び流れ応力などを計測した。得られた計測値を無負荷の円板から同様に採取した値と比較した結果、通過圧縮波の強さや材料に応じて、硬度、引張強度及び流れ応力の重大な上昇と伸び･延性の特徴的な変化が明らかになった。これらの結果は、同一材円筒の爆発実験と分裂モデルから得られた分裂エネルギーのひずみ速度依存性に、この先行圧縮効果を考慮に入れるために有効に適用された。

熊本大学大学院自然科学研究科機械システム工学部門　〒860-8555　熊本市黒髪2-39-1
†Corresponding address: hiroe@gpo.kumamoto-u.ac.jp